Journal of Materials Chemistry A

Accepted Manuscript

ROYAL SOCIETY OF CHEMISTRY

www.rsc.org/materialsA

J. Mater. Chem. A.

RSCPublishing

COMMUNICATION

Cite this: DOI: 10.1039/x0xx00000x
Received 00th January 2012,
Accepted 00th January 2012
DOI: 10.1039/x0xx00000x
www.rsc.org/

Fullerene imposed high open-circuit voltage in efficient perovskite based solar cells

*Lidón Gil-Escrig, MªCristina Momblona, Michele Sessolo and Henk J. Bolink**

Five different commercially available fullerenes are evaluated as the hole blocking/electron transporting materials in p-i-n methylammonium lead iodide perovskite solar cells using a vacuum deposited perovskite absorber layer. A significant enhancement of the solar cell performance can be obtained by selecting the proper fullerene derivative. Open-circuit voltages as high as 1.11 volts are obtained leading to power conversion efficiencies of 14.6 %.

Organometal halide perovskites have recently aroused much interest in photovoltaic applications because of their impressive performance, now exceeding 21%.[1-3] Several methods have been reported in order to deposit the perovskite layer; one of them is the physical vapour deposition technique. This presents some advantages over solution-based methods, such as high purity, compatibility with large area, and fine control over film thickness and morphology, leading to high-efficiency photovoltaic devices.[4-9] In general, two main device architectures have been used to fabricate perovskite solar cells. One of them (n-i-p) derives from cells built on a mesoporous TiO_2 scaffold with a typical configuration of substrate/TiO_2 (n)/ perovskite (i)/organic semiconductor (p).[10-13] The other configuration is the p-i-n structure, substrate/hole transporting layer (HTL) (p)/perovskite (i)/electron transporting layer (ETL)(n), in which the perovskite crystals are created on top of a transparent substrates covered with a hole transport layer, mostly poly(3,4-ethylenedioxythiophene) doped with poly(styrenesulfonate) (PEDOT:PSS). The ETL materials used in this configuration are mostly fullerene derivatives.[5, 14-16] *Jeng et al*. were the first in using three fullerene derivatives (C_{60}, phenyl-C_{61}-butyric acid methyl ester ($PC_{61}BM$), and indene-C_{60} bisadduct ($IC_{60}BA$) in a p-i-n configuration as ELTs.[14] They reported a PCE of 3.9% by employing PCBM and they verified the formation of a donor-acceptor interface at the $CH_3NH_3PBI_3/C_{60}$ interface. Soon after, *Sun et al* demonstrated a pure bilayer $CH_3NH_3PBI_3/PC_{60}BM$ solar cell with a performance with a PCE of 7.4%, the best reported until then for an all-solution-processable planar heterojunction device.[17] More recently, *Seok et al* reported the fabrication of highly improved $MAPbI_3$ perovskite solar cell using a solvent engineering approach and varying PCBM layer thicknesses , leading to 14% in the optimum device.[18] Apart from PCBM, other fullerene derivatives have been used in perovskite solar cells. For example Wang et al reported a high fill factor (FF) using a double layer structure to passivate traps states consisting of $PC_{61}BM/C_{60}$ or $IC_{60}BA/C_{60}$.[19] Also Chiang et al reported an efficiency of 16.3% using $PC_{71}BM$ as an electron transport material, in which solvent annealing of this layer was carefully conducted.[20] Recently, Jen et al demonstrated that the performance of a device follow the trend of increased electron mobility in the fullerene layer. They claimed that a higher electron mobilities of the fullerene film promotes charge dissociation/transport in the device. They reported efficiencies of 8.06%, 13.37% and 15.44% for $IC_{60}BA$, $PC_{60}BM$, C_{60}, respectively, as the mobility in C_{60} is higher than in the $PC_{60}BM$ and in the $IC_{60}BA$ films, respectively.[21] A lot of work on interface engineering between the PCBM layer and the metal contact has been carried out to overcome the mismatch in the energy levels of the metal contact (Al, Ag or Au) and the PCBM layer. In order to improve this, additional layers have been inserted between them, such as thermally evaporated LiF,[18] Ba[22] and C60/Bathocupraine (BCP),[23] or solution processed poly[(9,9-bis(30-(N,N-dimethylamino)propyl)-2,7-luorene)-alt-2,7-(9,9-dioctylfluorene)](PFN)[24], Bis-C60-surfactant,[25] TiO_x,[15] ZnO,[26] etc. PCBM is the most used fullerene derivative in the p-i-n architecture, yet its room temperature solubility in aromatic solvents is limited to approximately 20 mg/ml limiting the achievable layer thickness. Recently, different alkyl esters, instead of the methyl ester were offered commercially by Solenne BV. Additionally, two different alkyl esters of a slightly different fullerene employing a different linker were reported as having improved solubility and when used in an organic solar cell to cause higher open-circuit voltages (V_{oc}'s). *Sieval et al.* claimed that these two new fullerene derivatives combine the advantages of [60]PCBM, i.e., good solubility and easy

separation, with higher V_{oc} values due to slightly lower reduction potentials.[27]

Most p-i-n type perovskite solar cells, use PEDOT:PSS as the hole transporting layer yet as it is oxidized it does not block electrons. We have extensively studied the use of a thin electron blocking layer polyTPD (poly(N,N′-bis(4-butylphenyl)-N,N′-bis(phenyl)benzidine) (a hole transporting arylamine based polymer) in between the PEDOT: PSS and the perovskite absorber.[5, 28-32] As the polyarylamine layer is apolar, wetting from perovskite precursor solvents such as dimethylformamide is not good complicating the processing from the perovskite layer using precursor solutions. However, when the perovskite layer is deposited using vacuum based process, which is rather insensitive to the substrate layer, a homogeneous perovskite layer is formed on the electron blocking layer. Using this architecture Lin et al, achieved efficiencies of 16.5 % in optimized cells using PCBM and a p-type polymeric semiconductor as the electron blocking layer.[6]

In this communication, five different commercially available fullerenes are evaluated as the hole blocking/electron transporting materials in p-i-n perovskite solar cells employing polyTPD as the electron blocking layer with a vacuum deposited perovskite absorber layer. The fullerenes are members of two distinct families; [6,6]-phenyl-C_{61}-butyric acid with methyl (PCBM), butyl (PCBH), hexyl ester (PCBB) and iso-indene-C_{61} butyl (IPB) and hexyl ester (IPH) (Figure 1A). Improved processing and high power conversion efficiencies were obtained ranging from 13% to 14.6% depending on the particular fullerene employed. Hence, a significant enhancement of the solar cell performance can be obtained by selecting the proper fullerene derivative.

Device preparation

Materials: photolithographically patterned ITO covered glass substrates were purchased from Naranjo-Substrates (www.naranjosubstrates.com). PEDOT:PSS (Clevious PVP Al 4083) were obtained from Heraeus Holding used as received. Poly-TPD was purchased from ADS dyesource. PbI_2 was purchased from Aldrich and CH_3NH_3I from Lumtec, both were used as are. All the fullerenes (PCBM,PCBB,PCBH,IPB,IPH) was purchase from Solenne BV. Devices (Fig.1a) were prepared on cleaned ITO substrates, by spin coating a thin layer (70 nm) of PEDOT:PSS. On top of this a thin film of polyTPD was deposited from a chlorobenzene solution (7 mg/ml). The substrates were transferred to a vacuum chamber into a nitrogen-filled glovebox. (MBraun ,< 0.1 ppm O_2 and < 0.1 ppm H_2O) and evacuated to a pressure of $1x10^{-6}$ mbar. Two ceramic crucibles were filled with CH_3NH_3I and PbI_2 each which were heated to 70ºC and 250 ºC, respectively, the $CH_3NH_3PbI_3$ was then thermally evaporated to a thickness of 320nm, using a protocol described previously,[5] The film thickness was controlled by the PbI_2 evaporation rate maintained around 0.5 Å/s. The fullerene layer was deposited using a chlorobenzene solution of 20 mg/ml in ambient conditions using spin coating. The devices were completed by the thermal evaporation of the metal electrode under a base pressure of $2x10^{-6}$ mbar to a thickness of 10 nm of Ba and 100 nm of Ag. Device characterization was performed using a mini-sun simulator with a halogen lamp designed by ECN and calibrated with a Si reference cell. The unencapsulated solar cells were measured in a N_2-filled glovebox. The current density (J) versus voltage (V) characteristics were collected in the dark and under illumination using a shadow mask to prohibit lateral current collection from outside the active area. The current-density-versus-voltage (J-V) and irradiance-versus-voltage (L-V) characteristics were collected using keithley Model 2400 source measurement unit and a Si-photodiode coupled to an integrated sphere, respectively.

Results and Discussion

The crystallinity of the vacuum deposited perovskite was investigated by grazing incidence X-ray diffraction (GIXRD) measurements, revealing the pattern (in terms of both peak position and relative intensity) see Figure S1. The absorption spectrum of the perovskite film (Figure S2) is also typical which confirms the formation of the perovskite films. The main difference between PCBM and the PCB-Cn (PCBH and PCBB) are the increased length of the alkyl chains (Cn) used in the ester group that makes them more soluble. This leads to improved processing and to more homogeneous layers on top of the perovskite layer with fewer defects as evidenced by optical microscope images (Fig S3 in the supporting information). The film morphology on a micrometer scale as observed from atomic force microscope characterization does not show significant differences between the different fullerene derivatives (Figure S4). In all cases the fullerene films on top of the perovskite absorbers are rather smooth with a root-mean-square of around 10nm. The absorption spectra of the PCB-R films are similar, yet differ from the films of the IP-R derivatives (Figure 2).

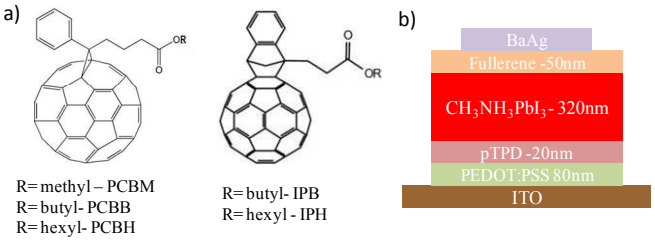

Fig. 1. (a) Chemical structures of the n-type fullerene derivatives, PCBM, PCBH, PCBB, IPB, IPH. (b) Device layout.

The PCB-R show a higher absorption (350-450 nm), with weak tails extending as far as 600 nm (Fig S5). The origin of this absorption tail is the result of light scattering or other experimental artefact. We note that films of C_{60} are reported as having similar absorption tails at low energies.[33] The IP-R films have only one absorption peak with a maximum around 325 nm whereas the PCB-R films present two peaks with maxima at 300 and 350 nm, due to the differences in the chemical structure as seen before of the fullerenes.

Journal of Material Chemistry A.

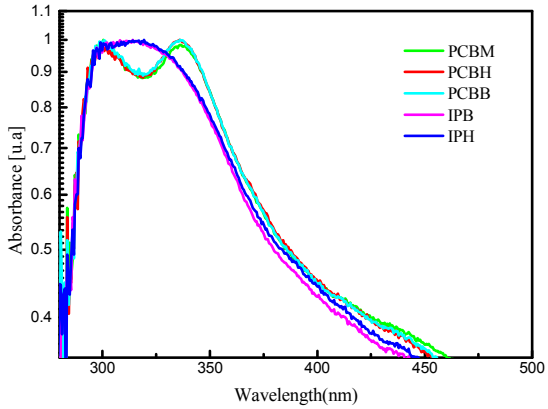

Fig. 2. **Optical absorption spectra for thin films on quartz of the five different fullerene derivatives.**

The devices employing the different fullerenes were characterized by determining the current density versus voltage both in the dark and under approximate 1 sun illumination. Figure 3a shows the dark current density versus voltage curves. The leakage current is low, indicating the high quality of the diodes independent on the fullerene employed for the whole series of devices. This is remarkable in view of the craters observed in the PCBM films (Fig S3) when deposited on top of the perovskite layer. It implies that such craters do not lead to ohmic leakage currents due to charge injection from the Ba/Ag electrode to the perovskite layer. A low leakage current density is beneficial for maximum open circuit voltages as the recombination due to leakage is diminished. The typical diode performance under approximately 1 sun illumination for the series of devices is shown in Figure 3b. In line with the good diode quality the J-V curves under illumination are also rather squared showing good charge extraction up to voltages close to V_{oc}. This is evidenced by the high fill factors obtained which are in between 75 and 80% (see Table 1). No clear trends in the FF with the different fullerenes employed were observed, although the devices with the PCBB fullerene showed consistently lower values than the others. The short-circuit current density (J_{sc}) of the solar cells was highest for the devices employing IPH as the n-type layer. There was not much difference in J_{sc} for the other devices employing the rest of the fullerenes, although the lowest J_{sc}'s were obtained for devices employing PCBM. In the devices using PCBM the reduction in current density is most likely due to the defects (craters) in the PCBM layer (see Figure S3) as commented previously. These defects are positions in the device that lead to charge recombination.

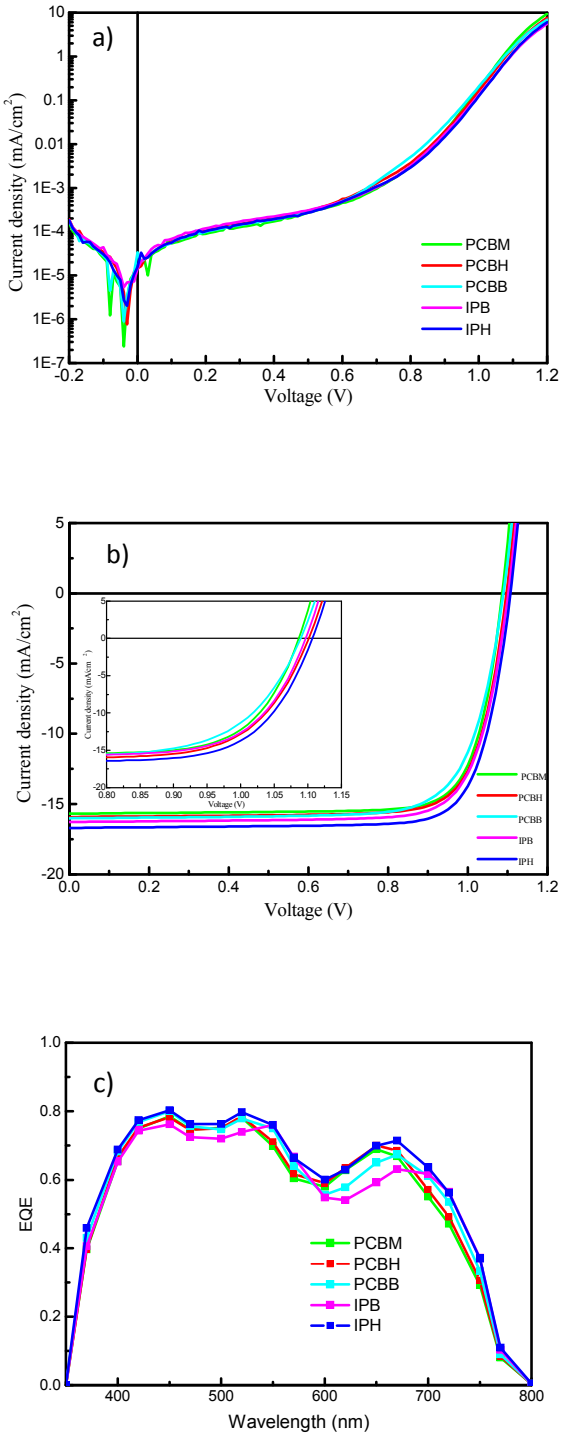

Fig. 3. Electrical characterization of the different diodes, (a) current density versus voltage plotted on a semilog scale (b) current density versus voltage curves under 1 sun illumination, inset shows amplification of the curves, and (c) external quantum efficiency (EQE_{PV}) of the different diodes.

The V_{oc} values obtained were higher (10-20 mV) for the devices employing the IP-R derivatives. This is in line with the lower reduction potential of the IP-R fullerenes compared to PCBM as reported by *Sieval et al.* [27] Hence, here a clear effect of the LUMO

level of the fullerene on the obtainable V_{oc} is shown, implying that further optimizations are possible. Due to both the higher current density and open circuit voltage for the devices using IPH as the hole blocking material, these devices exhibit the best power conversion efficiencies reaching 14.6 % for the record cell. Considering that the thickness of the perovskite layer used is 320 nm these efficiencies are among the best obtained for p-i-n type solar cells. No hysteresis was detected when a scan speed of 0.01 V/s was used for any of the devices using the different fullerenes. The forward and reverse J-V scans are virtually identical (Figure S6). The key device parameters are summarized in Table 1 (best data, represented) whereas the spreading of the data is represented in Figure S7 of the Supporting Information.

The external quantum efficiency (EQE_{pv}, Fig.3c) of the diodes, was determined by illuminating them with a white-light halogen lamp in combination with small bandpass filters. The EQEpv's of the devices employing the different fullerenes were high (0.7 to 0.8) in the visible range, while they diminished at wavelengths > 600nm, where the perovskite is weakly absorbing (EQEpv~0.6). The onset response lies in the near-infrared, 770nm. The trend in EQEpv is the same as previously observed for the J_{sc}, hence again the highest values are observed for the devices using IPH as the hole blocking material. The calculated current density is within 5 % of the measured value under 1 sun illumination.

Table 1. Photovoltaic parameters for the devices using the studied fullerenes.

Fullerene	V_{oc} (mV)	J_{sc} (mA/cm²)	*FF* (%)	*PCE* (%)
PCBM	1087	15.68	80	13.58
PCBH	1097	15.92	79	13.75
PCBB	1090	16.02	76	13.27
IPB	1102	16.28	78	14.02
IPH	1107	16.70	79	14.64

The increase in V_{oc} of the solar cells employing IPH, compared to those that use PCB-R varieties, may be due to the lower reduction potential of IPH. Yet this implies also that the quasi fermi level splitting in the perovskite layer must be sufficient to yield such a high V_{oc}. One of the major loss factors in the potential energy of the separated electron and holes is non-radiative decay.[34] Hence, if the V_{oc} is increased this may be related to a decrease in the non-radiative recombination of charge carriers in favour of radiative recombination. To test this, the diodes series containing the different fullerene derivatives were also driven under forward bias at moderate voltages (above the V_{oc}). The radiance was monitored using a sensitive Si-photodiode coupled to an integrating sphere.

In Figure 4a, the current density and irradiance as a function of the applied bias for all devices using the different fullerene derivatives is presented. A deviation from the leakage current occurs around 0.5 V, after which two regimes can be identified. First, an almost linear increase (in the log scale plot) is present, followed by a slower increase at higher voltages. The first regime is due to a diffusion current, whereas the second regime is indicative of an injection or space-charge limited current. Eventually, the current density reaches values higher than 100 mA/cm^2 at 2.5V, indicative of low carrier injection barriers and good charge transport in the diodes. Intense radiance was observed in all the devices prepared, but with only slight differences as a function of the fullerene derivative used. The turn-on voltage for the electroluminescence was found to be as low as 1 V for the complete series of devices, similar as previously reported.[22, 35, 36]

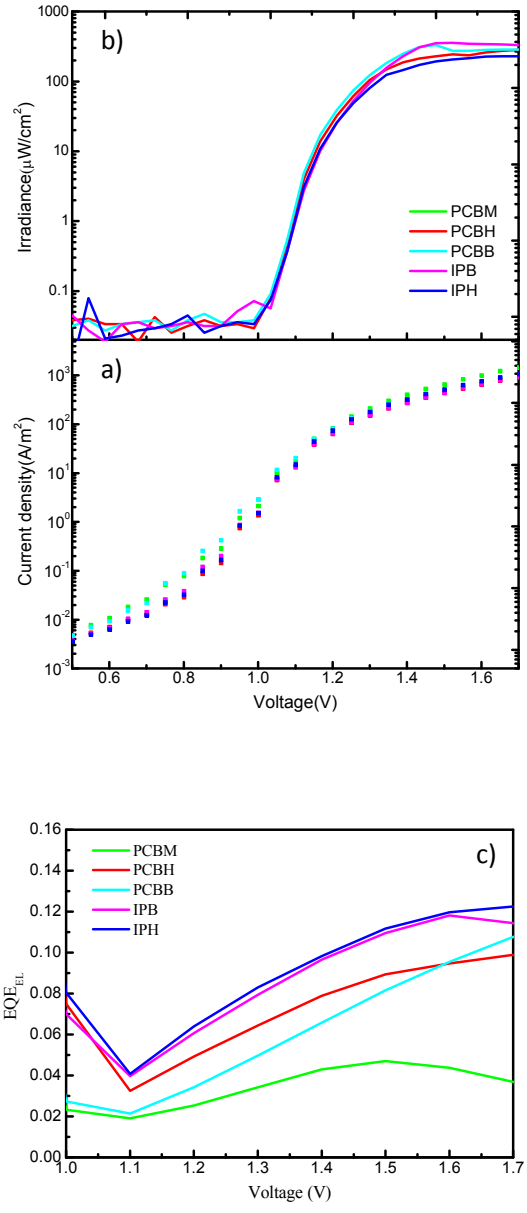

Fig. 4. (a) Current density and (b) radiance versus the voltage applied. (c) External quantum efficiency (EQE) versus de voltage applied for the different fullerene derivatives used.

The maximum external quantum efficiency of the electroluminescence (EQE_{EL}) of the diodes, however, did change depending on the fullerene derivative that was used. For the diode using PCBM an EQE_{EL} ~0.04% (Fig.4b) was obtained, very similar to that reported previously for similar diodes.[22, 35, 36] Yet the EQE_{EL} for the devices using fullerenes different from PCBM is increased, with the best values found for devices using the IP-R fullerenes, reaching 0.12 %. This is a 3 times increase compared to the EQE_{EL} of the diode employing PCBM. Hence, the increase in Voc of the solar cells is accompanied by an increase in the radiative efficiency most likely in part due a reduced non-radiative decay.

Conclusions

In summary, five different fullerene derivatives (PCBM, PCBH, PCBB, IPB and IPH) were evaluated as the electron transporting/hole blocking layer in p-i-n solar cells. The fullerenes with alkyl esters longer then methyl lead to improved layers with fewer defects than the layers obtained with PCBM. In the devices employing the PCB-R fullerenes, the improved layer quality did not lead to a significant improvement in photovoltaic behaviour. The devices that use the IP-R type fullerenes both the current density and open circuit voltage is improved, leading to improved photovoltaic performance of these devices. When operated as LEDs, it was shown that the external quantum efficiency of electroluminescence is improved for all devices with the longer alkyl ester fullerenes, which is indicative of a reduction in the non-radiative decay in these devices. Hence, the PCB-R and in particular IP-R are very promising fullerenes for perovskite solar cells including for larger area processing where the layer formation is more critical than in the small area devices used here.

Notes and references

Instituto de Ciencia Molecular, Universidad de Valencia, c/Catedrático J. Beltrán, 2, 46980 Paterna, Spain. E-mail: henk.bolink@uv.es; Fax: +34-963543273; Tel: +34-963544416

Acknowledgements

This work was supported by the European Union H2020 project INFORM (grant 675867), the Spanish Ministryof Economy and Competitiveness (MINECO) (MAT2014-55200)and the Generalitat Valenciana (Prometeo/2012/053).

References

1. A. Kojima, K. Teshima, Y. Shirai and T. Miyasaka, *J.Am. Chem.Soc.*, 2009, 131, 6050-6051.
2. M. M. Lee, J. Teuscher, T. Miyasaka, T. N. Murakami and H. J. Snaith, *Science*, 2012, 338, 643-647.
3. W. S. Yang, J. H. Noh, N. J. Jeon, Y. C. Kim, S. Ryu, J. Seo and S. I. Seok, *Science*, 2015, 348, 1234-1237.
4. M. Liu, M. B. Johnston and H. J. Snaith, *Nature*, 2013, 501, 395-398.
5. O. Malinkiewicz, A. Yella, Y. H. Lee, G. M. Espallargas, M. Graetzel, M. K. Nazeeruddin and H. J. Bolink, *Nat Photon*, 2014, 8, 128-132.
6. Q. Lin, A. Armin, R. C. R. Nagiri, P. L. Burn and P. Meredith, *Nat Photon*, 2015, 9, 106-112.
7. C.-W. Chen, H.-W. Kang, S.-Y. Hsiao, P.-F. Yang, K.-M. Chiang and H.-W. Lin, *Adv. Mater.*, 2014, 26, 6647-6652.
8. L. E. Polander, P. Pahner, M. Schwarze, M. Saalfrank, C. Koerner and K. Leo, *APL Materials*, 2014, 2, 081503.
9. L. K. Ono, M. R. Leyden, S. Wang and Y. Qi, *J.Mater.Chem.A*, 2016, DOI: 10.1039/C5TA08963H.
10. S. D. Stranks, G. E. Eperon, G. Grancini, C. Menelaou, M. J. P. Alcocer, T. Leijtens, L. M. Herz, A. Petrozza and H. J. Snaith, *Science*, 2013, 342, 341-344.
11. G. E. Eperon, V. M. Burlakov, P. Docampo, A. Goriely and H. J. Snaith, *Adv.Funct. Mater*, 2014, 24, 151-157.
12. B. Conings, L. Baeten, C. De Dobbelaere, J. D'Haen, J. Manca and H.-G. Boyen, *Adv.Mater*, 2014, 26, 2041-2046.
13. Q. Chen, H. Zhou, Z. Hong, S. Luo, H.-S. Duan, H.-H. Wang, Y. Liu, G. Li and Y. Yang, *J.Am.Chem.Soc*, 2014, 136, 622-625.
14. J.-Y. Jeng, Y.-F. Chiang, M.-H. Lee, S.-R. Peng, T.-F. Guo, P. Chen and T.-C. Wen, *Adv. Mater.*, 2013, 25, 3727-3732.
15. P. Docampo, J. M. Ball, M. Darwich, G. E. Eperon and H. J. Snaith, *Nat Commun*, 2013, 4.
16. J.-Y. Jeng, K.-C. Chen, T.-Y. Chiang, P.-Y. Lin, T.-D. Tsai, Y.-C. Chang, T.-F. Guo, P. Chen, T.-C. Wen and Y.-J. Hsu, *Adv.Mater*, 2014, 26, 4107-4113.
17. S. Sun, T. Salim, N. Mathews, M. Duchamp, C. Boothroyd, G. Xing, T. C. Sum and Y. M. Lam, *Energy Environ.Scie*
18. J. Seo, S. Park, Y. Chan Kim, N. J. Jeon, J. H. Noh, S. C. Yoon and S. I. Seok, *Energy Environ.Scie*, 2014, 7, 2642-2646.
19. Q. Wang, Y. Shao, Q. Dong, Z. Xiao, Y. Yuan and J. Huang, *Energy Environ.Scie*, 2014, 7, 2359-2365.
20. C.-H. Chiang, Z.-L. Tseng and C.-G. Wu, *J.Mater.Chem.A*, 2014, 2, 15897-15903.
21. P.-W. Liang, C.-C. Chueh, S. T. Williams and A. K. Y. Jen, *Adv.Energy Mater*, 2015, 5, n/a-n/a.
22. L. Gil-Escrig, G. Longo, A. Pertegas, C. Roldan-Carmona, A. Soriano, M. Sessolo and H. J. Bolink, *Chem.Comm*, 2015, 51, 569-571.
23. Z. Xiao, C. Bi, Y. Shao, Q. Dong, Q. Wang, Y. Yuan, C. Wang, Y. Gao and J. Huang, *Energy Environ.Scie*, 2014, 7, 2619-2623.
24. J. You, Y. Yang, Z. Hong, T.-B. Song, L. Meng, Y. Liu, C. Jiang, H. Zhou, W.-H. Chang, G. Li and Y. Yang, *Appl.Phys.Lett*, 2014, 105, 183902.
25. P.-W. Liang, C.-Y. Liao, C.-C. Chueh, F. Zuo, S. T. Williams, X.-K. Xin, J. Lin and A. K. Y. Jen, *Adv.Mater*, 2014, 26, 3748-3754.
26. W. Qiu, M. Buffière, G. Brammertz, U. W. Paetzold, L. Froyen, P. Heremans and D. Cheyns, *Org.Electron*, 2015, 26, 30-35.
27. A. B. Sieval, N. D. Treat, D. Rozema, J. C. Hummelen and N. Stingelin, *Chem.Comm*, 2015, 51, 8126-8129.
28. K. Tvingstedt, O. Malinkiewicz, A. Baumann, C. Deibel, H. J. Snaith, V. Dyakonov and H. J. Bolink, *Sci. Rep.*, 2014, 4, 6071.
29. C. Roldan-Carmona, O. Malinkiewicz, A. Soriano, G. Minguez Espallargas, A. Garcia, P. Reinecke, T. Kroyer, M. I. Dar, M. K. Nazeeruddin and H. J. Bolink, *Energy Environ.Scie*, 2014, 7, 994-997.
30. C. Roldan-Carmona, O. Malinkiewicz, R. Betancur, G. Longo, C. Momblona, F. Jaramillo, L. Camacho and H. J. Bolink, *Energy Environ.Scie*, 2014, 7, 2968-2973.
31. C. Momblona, O. Malinkiewicz, C. Roldán-Carmona, A. Soriano, L. Gil-Escrig, E. Bandiello, M. Scheepers, E. Edri and H. J. Bolink, *APL Mat.*, 2014, 2, 081504.
32. O. Malinkiewicz, C. Roldán-Carmona, A. Soriano, E. Bandiello, L. Camacho, M. K. Nazeeruddin and H. J. Bolink, *Adv.Ener.Mater.*, 2014, DOI: 10.1002/aenm.201400345, 1400345.
33. S. Cook, H. Ohkita, Y. Kim, J. J. Benson-Smith, D. D. C. Bradley and J. R. Durrant, *Chem.Phys.Lett*, 2007, 445, 276-280.
34. O. D. Miller, E. Yablonovitch and S. R. Kurtz, *Photovoltaics, IEEE Journal of*, 2012, 2, 303-311.
35. Z.-K. Tan, R. S. Moghaddam, M. L. Lai, P. Docampo, R. Higler, F. Deschler, M. Price, A. Sadhanala, L. M. Pazos, D. Credgington, F. Hanusch, T. Bein, H. J. Snaith and R. H. Friend, *Nat Nano*, 2014, 9, 687-692.
36. Y.-H. Kim, H. Cho, J. H. Heo, T.-S. Kim, N. Myoung, C.-L. Lee, S. H. Im and T.-W. Lee, *Adv.Mater*, 2015, 27, 1248-1254.

TOC graphic